Energy 262 (2023) 125271

Contents lists available at ScienceDirect

Energy

journal homepage: www.elsevier.com/locate/energy

Multi-objective simulation–optimization via kriging surrogate models applied to natural gas liquefaction process design

Lucas F. Santos [a,b,*], Caliane B.B. Costa [a], José A. Caballero [b], Mauro A.S.S. Ravagnani [a]

[a] Department of Chemical Engineering, State University of Maringá, Avenida Colombo 5790, 87020900, Maringá, Brazil
[b] Institute of Chemical Process Engineering, University of Alicante, Ap. Correos 99, 03080, Alicante, Spain

ARTICLE INFO

Keywords:
Multi-objective simulation–optimization
Natural gas liquefaction
Surrogate-based optimization
Process design
Kriging
Mathematical programming

ABSTRACT

A surrogate-based multi-objective optimization framework is employed in the design of natural gas liquefaction processes using reliable, black-box process simulation. The conflicting objectives are minimizing both power consumption and heat exchanger area utilization. The Pareto solutions of the single-mixed refrigerant (SMR) and propane-precooled mixed refrigerant (C3MR) processes are compared to determine the suitability of each process in terms of energy consumption and heat exchanger area. Kriging models and the ε-constraint methodology are used to sequentially provide simple surrogate optimization subproblems, whose minimizers are promising feasible and non-dominated solutions to the original black-box problem. The surrogate-based ε-constrained optimization subproblems are solved in GAMS using CONOPT. The Pareto Fronts achieved with the surrogate-based framework dominate the results from the NSGA-II, a well-established meta-heuristics of multi-objective optimization. The objective functions of non-dominated solutions go as low as 1045 and 980.3 kJ/kg-LNG and specific *UA* values of 212.2 and 266.9 kJ/(°C kg-LNG) for SMR and C3MR, respectively. The trade-off solutions that present the minimum sum of relative objectives are analyzed as well as the dominance of C3MR over SMR at low power consumption values and conversely at low heat exchanger area utilization.

1. Introduction

Multi-objective optimization is a key to success in engineering design when the decision-making process involves multiple, competing objectives. However, to use optimization techniques in those tasks, models that describe the considered system are required. For complex chemical processes, modular-sequential process simulators (flowsheeting programs) are often resorted as simulated models. These programs provide accurate predictions for a variety of processes by using rigorous thermodynamic and unit operation models and numerical methods. The motivating problem for this work is the design of natural gas liquefaction processes considering the conflicting goals of minimizing both power consumption and heat transfer area utilization. The main challenge that makes the use of modular-sequential process simulators attractive in this application is modeling the multi-stream heat exchangers (MSHEs). That is especially the case because the streams in these heat exchangers undergo phase transitions, and their compositions and flow rates vary as they are design variables. There are attempts in the literature to model the MSHEs with algebraic formulation using Generalized Disjunctive Programming for dealing with phase change [1], superstructure-based approach [2], and nondifferentiable models explicitly [3]. In the present work, the advantages and disadvantages of using black-box process simulators are dealt with and elaborated.

Some challenges come from embedding such simulated, or implicit, models into optimization problems. The simulator-dependent black-box functions are by definition not available in symbolic form, which prevents the use of deterministic global optimization [4]. Derivatives have to be estimated using numerical differentiation via perturbation of independent variables. These functions can be noisy due to round-off and numerical convergence tolerance [5]. Such noise is usually negligible for simulation, but it can hamper the calculation of accurate derivatives for gradient-based optimization methods. In addition, the computational effort to evaluate these functions is not negligible. This prohibits optimization approaches that require lots of function evaluations like second-order methods that use hessian information, for example. Finally, the black-box aspect of the model hides from the user important information from the algebraic model such as nondifferentiabilities, which is notably the case for MSHEs [3].

Multi-objective simulation–optimization (MOSO) problems can be defined as to determine a set of $\boldsymbol{x}^* \in \mathbb{R}^n$ that are non-dominated

* Corresponding author at: Institute of Chemical Process Engineering, University of Alicante, Ap. Correos 99, 03080, Alicante, Spain.
E-mail address: pg54347@uem.br (L.F. Santos).

https://doi.org/10.1016/j.energy.2022.125271
Received 25 March 2022; Received in revised form 28 July 2022; Accepted 23 August 2022
Available online 18 September 2022

solutions of the following:

$$\begin{aligned} \min_{\boldsymbol{x}\in\boldsymbol{D}} \quad & \boldsymbol{f}(\boldsymbol{x}) = \left[f_1(\boldsymbol{x}), \ldots, f_k(\boldsymbol{x})\right] \\ s.t. \quad & \boldsymbol{g}(\boldsymbol{x}) \leq 0. \end{aligned} \tag{MOSO}$$

The objectives $\boldsymbol{f} : \mathbb{R}^n \mapsto \mathbb{R}^k$ and constraints $\boldsymbol{g} : \mathbb{R}^n \mapsto \mathbb{R}^q$ are computationally-intensive, moderately noisy, black-box functions. k and q are the number of objectives and constraints, respectively, and n is the dimension of $\boldsymbol{x}$. Since the noise is neglected for function evaluation, the expected value of these functions are approximated to the simulated value.

A suitable application for the Problem (MOSO) is the optimal design of LNG processes considering conflicting goals. The purpose of such processes is to cool the natural gas stream to −160 °C using refrigeration cycle(s) so it is liquefied at atmospheric pressure. These processes are mandatory for the natural gas safe and efficient commercialization and transportation through long distances, *i.e.* when the natural gas resources are far apart from the end consumer [6]. This energy-intensive part of the LNG supply chain is responsible for 40%–60% of the cost of the final project [7]. For that, energy optimization of LNG processes have been extensively studied in the past [8]. However, the energy-optimum design solution without heat exchanger area limit might not be appropriate [9]. That is because the optimum design of these processes presents a clear trade-off between energy consumption and equipment size [10]. The concern of achieving high energy efficiency and diminished equipment size is further emphasized in offshore processes, where the plant site size is significantly restricted.

Although there is a vast literature on single-objective optimization of natural gas liquefaction processes, the evaluation of optimal trade-off in these processes' design has been timidly addressed. Khan et al. [10] applied multi-objective optimization to the dual-mixed refrigerant LNG process. The BOX optimization method was used to minimize separately the specific compression power and the heat exchanger area. The authors identified that these objectives are competing ones, and they used the non-dominated sorting genetic algorithm version two (NSGA-II [11]) implemented in the "gamultiobj" function from MATLAB to deal with balancing the objectives. Ghorbani et al. [12] used Genetic Algorithms (GAs) for single and multiple objectives to optimize the propane-precooled mixed-refrigerant (C3MR) LNG process. The competing goals of maximizing exergy efficiency and minimizing total product cost were considered. A trade-off non-dominated solution was determined with 7.25 $/h of product cost and 50.71% exergy efficiency. Song et al. [13] optimized the nitrogen expansion LNG process with carbon dioxide expansion precooling. The authors used a simple GA to individually minimize the specific energy consumption and maximize the liquefaction rate. The multi-objective scenario was considered using the NSGA-II and increased the liquefaction rate from 0.77 to 0.81, while diminishing the energy consumption by 10.1% compared to a base case.

Nguyen et al. [14] provided an interesting comparison of the single-mixed refrigerant (SMR), single-expander, and dual-expander LNG processes considering the trade-off between power consumption and heat exchanger area. A multi-objective GA was employed for the optimization, and different natural gas compositions were considered. Their findings indicate that the SMR is more energetically efficient at the price of having increased heat exchanger area utilization and process complexity. Primabudi et al. [15] optimized the C3MR process considering exergy efficiency and total product cost objectives. The NSGA-II solver was applied and the Pareto feasible solutions are between 0.557 and 0.613 for exergetic efficiency and between 45600 and 52776 $/h for the total cost of the product. Mofid et al. [16] optimized the parallel nitrogen expansion LNG process using a multi-objective particle swarm optimization (PSO) algorithm in two scenarios. At design, the objectives of minimizing energy consumption and heat exchangers size were considered. At operation, the minimization of energy consumption and maximization of liquefaction rate, with fixed equipment size are performed. The non-dominated solutions of the multi-objective PSO approach dominated the base case and GA results.

The literature on multi-objective optimization of natural gas liquefaction processes is entirely based on meta-heuristics, namely NSGA-II and multi-objective PSO. Recent findings have shown that, to this class of simulation–optimization problems, surrogate-based approaches coupled with gradient-based optimization can perform better than state-of-the-art meta-heuristics, such as GA and PSO [17]. Consequently, frameworks based on surrogate models applied to the multi-objective problem in the design of LNG processes can improve the assessment of their competing objectives. This work's objective is to apply a multi-objective optimization framework based on surrogates to the optimal design LNG processes using reliable process simulators and considering competing objectives.

The proposed methodology is an adaptation of our previous work [17] to the multi-objective problem. This framework includes using kriging models to replace the black-box objectives functions and constraints and ε-constraint method to handle competing objectives. The surrogate optimization subproblems are embedded into a nonlinear programming problem and solved with CONOPT local solver in the General Algebraic Modeling System (GAMS). This paper embodies as case study the optimal design of the SMR and C3MR processes for natural gas liquefaction considering the minimization of both power consumption and heat transfer area utilization. The Pareto Front determined by the present approach is compared with results from NSGA-II, a well-established and highly employed meta-heuristic method in multi-objective optimization of LNG processes. Suitable trade-off solutions of the SMR and C3MR processes are analyzed. These processes are compared regarding dominance in the objective functions space, and their suitability is discussed. Therefore, the novelty of the present work is two-fold. First, to the best of the knowledge of the authors, this is the first application of multi-objective surrogate-based optimization to design natural gas liquefaction processes. Second, an in-depth comparison between the optima results of the SMR and C3MR processes is performed. The comparison assessment does not consider only the single-objective energy optimum of each process as it is usually performed in the literature. Instead, the Pareto solutions of these processes with respect to the competing objectives of power consumption and heat exchanger area utilization are compared and a dominance inflection point is derived.

2. Kriging-based multi-objective optimization

An extension to the single-objective kriging-based optimization approach in Santos et al. [17] is proposed to solve the multi-objective simulation–optimization problems as in Problem (MOSO). The present framework relies on kriging surrogate modeling, ε-constraint method, and gradient-based solver.

2.1. Kriging model

The data-driven, interpolating model called kriging is defined as the sum of a regression model and an estimated error. The latter is considered to be the realization of a Gaussian process that predicts the deviation between the regression model and the underlying function. It is assumed to have zero mean and covariance given by some spatial correlation function. Kriging models are derived to be the best linear unbiased predictors at unsampled points [18]. In other words, the kriging model interpolates the data, and the departure between regression and actual function is more correlated for points that are closer together in space than those that are far apart.

It is first considered that $\mathbf{X} = [\boldsymbol{x}^{(1)} \ldots \boldsymbol{x}^{(m)}]^T$, the set of m sampled points, and their output values

$$\mathbf{Y} = [\boldsymbol{f}(\boldsymbol{x}^{(1)}) \ldots \boldsymbol{f}(\boldsymbol{x}^{(m)});\ \boldsymbol{g}(\boldsymbol{x}^{(1)}) \ldots \boldsymbol{g}(\boldsymbol{x}^{(m)})]^T \tag{1}$$

are available. For smoothness of the surrogate models, the Gaussian correlation function is used as

$$\mathcal{R}(\boldsymbol{\theta}, \boldsymbol{x}^{(i)}, \boldsymbol{x}^{(j)}) = \exp\left[-\sum_{h=1}^{n} \boldsymbol{\theta}_h \left(x_h^{(i)} - x_h^{(j)}\right)^2\right]. \tag{2}$$

Given the data and correlation model, it is possible to define the matrix $\mathbf{R}(\boldsymbol{\theta}) \in \mathbb{R}^{m\times m\times(k+q)}$ of the correlation function evaluated at the sampled points for each objective and constraint, and the matrix $\mathbf{r}(\boldsymbol{x}, \boldsymbol{\theta}) \in \mathbb{R}^{m\times(k+q)}$ of the correlation function evaluated at an unsampled point and the data for each objective and constraint. Both $\mathbf{R}$ and $\mathbf{r}$ are functions of the correlation parameters $\boldsymbol{\theta} \in \mathbb{R}^{n\times(k+q)}$, which are defined by minimizing the log-likelihood of the model given the data of each function [19].

In the present work, the kriging models assume a constant regression term (ordinary kriging), such that the error model captures the behavior of the underlying function that generates the data. Considering the above-mentioned assumptions and following the derivation of kriging as the best linear unbiased predictor as in Santos et al. [19] for $\boldsymbol{f}$ and $\boldsymbol{g}$, these surrogates become

$$\hat{f}_i(\boldsymbol{x}) = \hat{\beta}_i + \mathbf{r}_i(\boldsymbol{x})^T \mathbf{R}_i^{-1}(\mathbf{Y}_i - \mathbf{1}\hat{\beta}_i), \quad i = 1, \ldots, k+q. \tag{3}$$

in which $\hat{\beta}_i = \mathbf{1}^T\mathbf{R}_i^{-1}\mathbf{Y}_i / \mathbf{1}^T\mathbf{R}_i^{-1}\mathbf{1}$, $i = 1, \ldots, k+q$ are the generalized least square solution of the ordinary kriging for each objective and constraint.

2.2. ε-constraint method

The ε-constraint method consists of selecting one objective to be optimized ($i = s$), while the others ($i \neq s$) are converted into constraints such that [20]

$$f_i \leq \varepsilon_i, \; i = 1, \ldots, k \mid i \neq s. \tag{4}$$

The multi-objective problem in Problem (MOSO) can be reformulated into an ε-single-objective simulation–optimization (ε-SO) one as follows:

$$\begin{aligned} \min_{\boldsymbol{x}\in\boldsymbol{D}} \; & f_s(\boldsymbol{x}) \\ s.t. \; & f_i(\boldsymbol{x}) \leq \varepsilon_i, \quad i = 1, \ldots, k \mid i \neq s \\ & \boldsymbol{g}(\boldsymbol{x}) \leq 0. \end{aligned} \tag{ε-SO}$$

Varying the values of ε_i yields non-dominated solutions of Problem (MOSO), forming the Pareto Front [21].

2.3. Multi-objective surrogate optimization problem

The kriging models defined in Eq. (3) are readily available in mathematical notation and can be implemented in specialized software, algebraic modeling language systems, to be solved with efficient gradient-based optimization tools [17]. Algebraically, these kriging models in Eq. (3) are

$$\hat{f}_i(\boldsymbol{x}) = \hat{\beta}_i + \sum_{j=1}^{m} \alpha_{j,i} \; e^{-\sum_{l=1}^{n} \theta_{l,i}(x_l - X_{j,l})^2}, \tag{5}$$

in which $\boldsymbol{\alpha}_{:,i} = \mathbf{R}_i^{-1}(\mathbf{Y}_i - \mathbf{1}\hat{\beta}_i)$. Notice that, the memory-intensive matrix $\mathbf{R}$ does not need to be stored. Instead, only $\boldsymbol{\alpha}$, $\boldsymbol{\theta}$, and $\mathbf{X}$ do.

Given the algebraic formulation of kriging model in Eq. (5), it is possible to rewrite the problem in Problem (ε-SO) into the ε-constrained surrogate optimization subproblem (ε-SBO) explicitly such as

$$\begin{aligned} \min_{\boldsymbol{x}\in\boldsymbol{D}, \tilde{f}_s} \; & \tilde{f}_s \\ s.t. \; & \tilde{f}_s = \hat{\beta}_i + \sum_{j=1}^{m} \alpha_{j,i} \; e^{-\sum_{l=1}^{n} \theta_{l,i}(x_l - X_{j,l})^2}, \quad i = s \\ & \hat{\beta}_i + \sum_{j=1}^{m} \alpha_{j,i} \; e^{-\sum_{l=1}^{n} \theta_{l,i}(x_l - X_{j,l})^2} \leq \varepsilon_i, \quad i = 1, \ldots, k \mid i \neq s \\ & \hat{\beta}_i + \sum_{j=1}^{m} \alpha_{j,i} \; e^{-\sum_{l=1}^{n} \theta_{l,i}(x_l - X_{j,l})^2} \leq 0, \quad i = k+1, \ldots, k+q. \end{aligned} \tag{ε-SBO}$$

The multi-objective surrogate optimization in Problem (ε-SBO) is an algebraic approximated substitute of the original black-box optimization in Problem (ε-SO). Its solution is a possibly feasible, Pareto optimal candidate of the original problem considering the ε value.

It is worth mentioning that in the nonlinear programming model in Problem (ε-SBO), $\boldsymbol{\theta}$, $\hat{\boldsymbol{\beta}}$, and $\boldsymbol{\alpha}$ are constant. The resulting surrogate problem has $n+1$ variables, which are $\tilde{f}_s$ and $\boldsymbol{x}$, and $k+q$ nonlinear constraints. Notice that the variable $\tilde{f}_s$ receives the residual of $\hat{f}_s(\boldsymbol{x})$ and is only necessary because some algebraic modeling systems, such as GAMS, solve for the minimization or maximization of a variable and not for the residual of an equation directly. Otherwise, $\hat{f}_s(\boldsymbol{x})$ would be consider as objective function and Problem (ε-SBO) resembling the definition of the Problem (ε-SO). Therefore, the present kriging-based framework transforms the multi-objective black-box optimization in Problem (MOSO) into simpler ε-constrained nonlinear programming problems solved sequentially to provide samples that are possible non-dominated solutions to the original problem.

3. LNG processes

The optimal design of the SMR and C3MR processes, considering the trade-off between energy consumption and equipment size are assessed as case study in the present work. These refrigeration processes use a mixture undergoing a thermodynamic cycle to produce a heat sink in the evaporation stage to liquefy the natural gas stream. The C3MR process adds a refrigeration cycle operating with pure propane that evaporates at different pressure levels precooling the natural gas and mixed refrigerant streams. Fig. 1 illustrates the process flow diagrams of both the SMR and the C3MR.

The mixed-refrigerant cycle employs a compression system with four stages, considering coolers in between compressors and flash separators for recovering the liquid phase. The refrigerant condensate is sub-cooled in the MSHE-1 separately from the vapor phase, which is further cooled, liquefied, and possibly sub-cooled in the MSHE-2. These multi-component streams are mixed back inside the MSHE-1 in the cold pass, as represented in Fig. 1. A four-stage compression system is also considered in the propane cycle. The propane stream is expanded in valves at four pressure levels, and the resulting condensate is separated in the flash drums. The condensate streams are totally evaporated in different passes of the MSHE-100 to pre-cool the natural gas and mixed-refrigerant streams.

3.1. Process simulation

The rigorous process simulations are performed using Aspen HYSYS® V9, employing as thermodynamic package Peng–Robinson that is suitable for nonpolar mixtures like hydrocarbons and nitrogen. It is supplied to the liquefaction process a natural gas stream (NG) at 5000 kPa and 32 °C. In Table 1, the NG composition jointly with some process considerations and other simulation parameters following the literature [22] are presented. The NG mass flow rate is 1 kg/h as a basis of calculation. However, it does not loose of generality, once the results can be reproduced for different natural gas flow rates. That can be achieved by multiplying the extensive variables of refrigerant component mass flow rate, specific power consumption, and specific heat conductance (UA), to be presented later, by the factor of increase/decrease. The mixed-refrigerant refrigerant is composed of nitrogen, methane, ethane, propane, and i-pentane. Each component mass flow rate is a decision variable of the optimization problem. The heavy component i-pentane is considered only for the SMR to account for the cooling task at high temperatures as it increases the bubble point temperature of the mixture [23]. This is not required in the C3MR because that is achieved by the propane precooling cycle. The pressure of discharge and suction of the mixed-refrigerant cycle, P_{dis} and P_{suc}, are also decision variables, while the intermediate pressures come out of the constant pressure ratio assumption given by $(P_{dis}/P_{suc})^{1/4}$. The temperatures of hot streams leaving an MSHE are equal and set to the expansion temperature (stream 11l in SMR and 9l in C3MR) for MSHE-

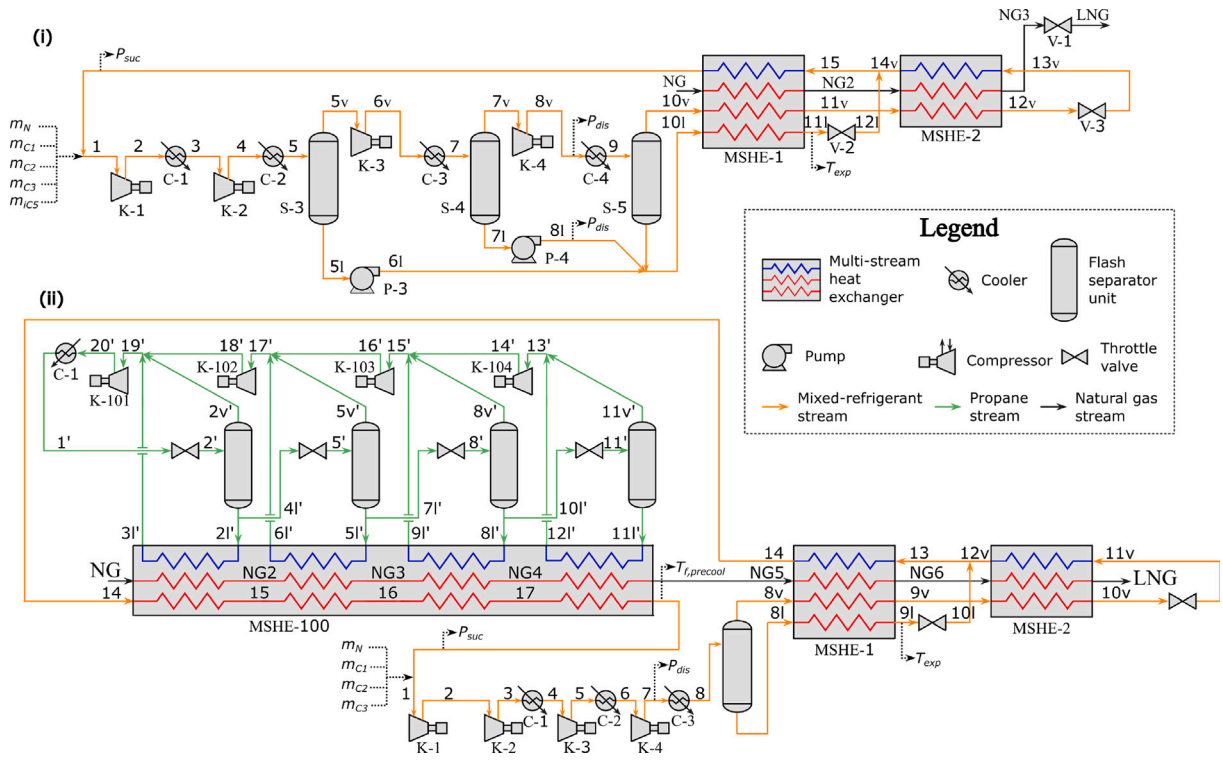

Fig. 1. Process flow diagram of (i) SMR and (ii) C3MR.

1, which is a design variable. To ensure the LNG requirements at the final pressure as exposed in Table 1, the temperature of −149.7 °C is fixed in the final expansion stage.

The propane cycle in the C3MR has some degrees of freedom that can be satisfied with the following assumptions. Setting discharge pressure (stream 20') to the minimum, while above saturation pressure of propane at 40 °C at stream 1'. This pressure is set to 1398 kPa. The propane streams leave MSHE-100 (3l', 6l', 9l', and 12l') as a saturated vapor at the same temperature of the inlet streams, such that only the heat of vaporization is used as heat sink. The propane streams enter MSHE-100 (2l', 5l', 8l', and 11l') 3 °C below the temperature of the cold-end hot streams (14, 15, 16, 17) to guarantee the minimum temperature driving force. The latter is calculated to achieve a constant temperature step at each pass of MSHE-100 that is $T_{14}-T_{f,precool}/4$. The final temperature of precooling cycle (stream 1 and NG5 in Fig. 1 (ii)) is a decision variable of the process optimization. Given these assumptions and decision variables, the precooling cycle is fully determined and the mass flow rate of propane, as well as the intermediate pressures of the cycle, come from the energy balances performed by the process simulator.

3.2. Process optimization

The goal of design in natural gas liquefaction processes is to reduce energy consumption while maintaining small pieces of equipment. Also, a minimum value of temperature difference between hot and cold streams all through the MSHE 1 and 2 has to be assured, once in MSHE-100 it is already specified as elaborated in Section 3.1. The kriging model, which is to be used to replace objectives and constraints, requires some degree of smoothness of the black-box functions, and that may not be the case for this constraint at every configuration of decision variables. In fact, the nonlinear behavior of enthalpy with temperature in mixtures, which is worsened by phase change, can cause a change in the pinch point location of the multi-stream heat exchanger. The change in the pinch location from a stream regime to another, *e.g.* from vapor to vapor and liquid or liquid phase, can cause an abrupt variation of the minimum temperature approach with respect to the decision variables. That is illustrated in the dashed lines of Fig. 2 with a sensitivity analysis around a carefully selected configuration of decision variables, where the non-smooth behavior of this constraint happens.

To overcome this issue, Santos et al. [17] propose to discretize the MSHEs 1 and 2 in $\kappa = 1, \ldots, K \times N_{MSHE}$ sections to make it more likely

Table 1
Simulation parameters and process considerations for the LNG processes, based on the available literature [22].

Natural gas feed condition	
Property	**Condition**
Temperature	32 °C
Pressure	5,000 kPa
Flow rate	1.0 kg/h
Composition	**Molar fraction**
Nitrogen	0.0022
Methane	0.9133
Ethane	0.0536
Propane	0.0214
i-Butane	0.0046
n-Butane	0.0047
i-Pentane	0.0001
n-Pentane	0.0001
Design parameters and considerations	
Temperature of intermediate cooling	40 °C
Cold utility temperature	30 °C
Pressure drop intermediate cooling	25.0 kPa
Molar vapor fraction of LNG	8.0%
Temperature of LNG	−158.6 °C
Pressure of LNG	120.0 kPa
Compressor adiabatic efficiency	0.75
Pump adiabatic efficiency	0.75
Thermodynamic package	Peng–Robinson
MSHE-100 pressure drop at each pass (hot stream)	25.0 kPa
MSHE-100 pressure drop at each pass (cold stream)	0.0 kPa
MSHE-1 and 2 pressure drop at each pass (hot stream)	50.0 kPa
MSHE-1 and 2 pressure drop at each pass (cold stream)	5.0 kPa
Minimum temperature approach	3 °C

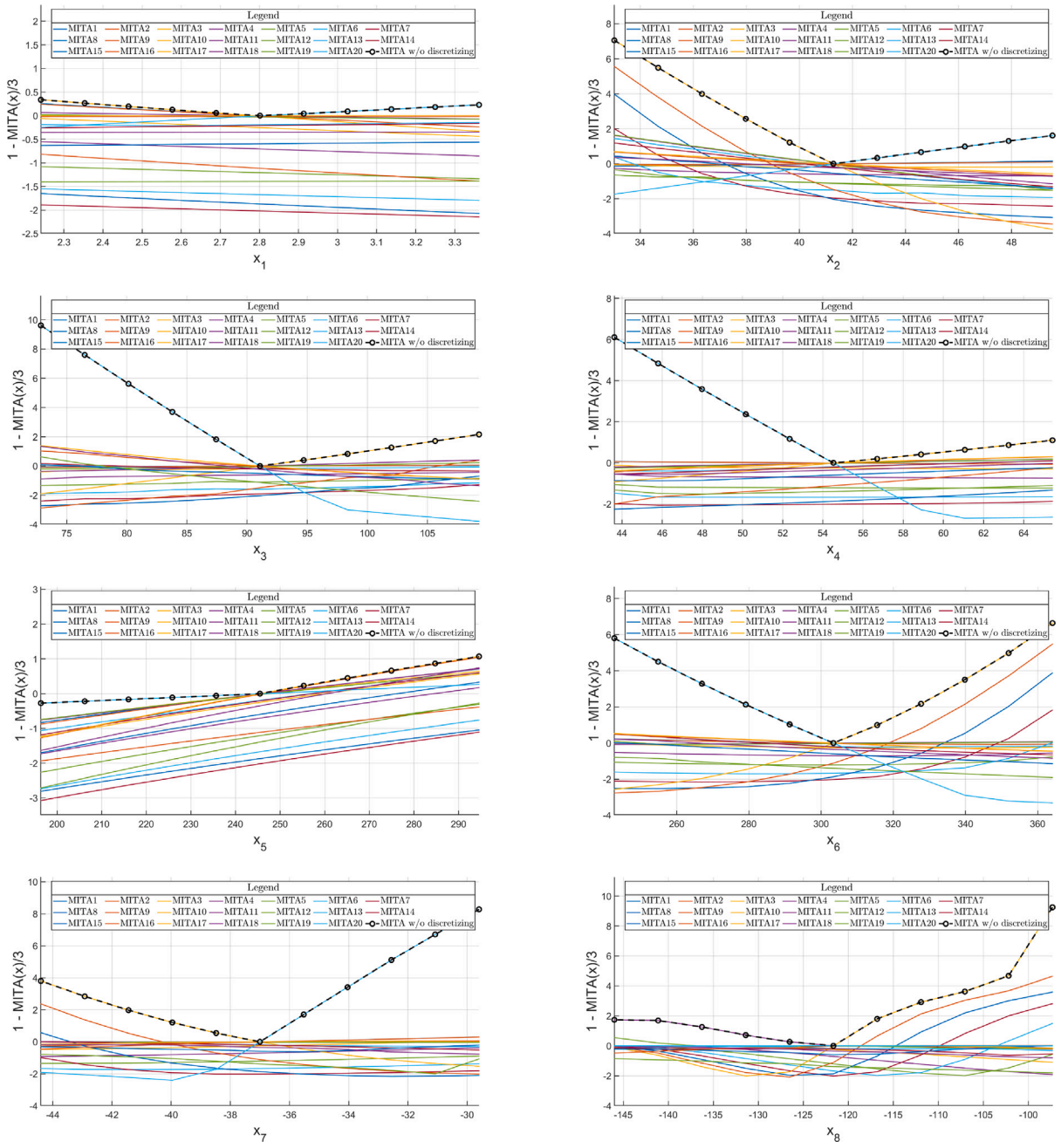

Fig. 2. Minimum temperature approach behavior with respect to $\boldsymbol{x}$ in the MSHEs with and without discretization.

that the temperature driving force constraints are smooth functions. K is the number of sections in each of the N_{MSHE} multi-stream heat exchangers. It is also illustrated in Fig. 2 with $K = 10$, for which it is possible to see that the $K \times N_{MSHE}$ functions (solid lines) are less stiff than the one without discretization (dashed line). The optimal process design can be formulated as the following multi-objective optimization problem

$$\begin{aligned} \min_{\boldsymbol{x}\in\boldsymbol{D}} \quad & \boldsymbol{f}(\boldsymbol{x}) = \left[\frac{\sum_{p\in PM} W_p(\boldsymbol{x})}{\dot{m}_{LNG}};\ \frac{\sum_{ex\in HE} UA_{ex}(x)}{\dot{m}_{LNG}} \right] \\ s.t. \quad & g_\kappa(\boldsymbol{x}) = 1 - \frac{\min_{\ell\in\Omega_\kappa} \left\{ Th_{\kappa,\ell}(\boldsymbol{x}) - Tc_{\kappa,\ell}(\boldsymbol{x}) \right\}}{3} \le 0, \quad \kappa = 1, \ldots, K \times Ne \\ & \boldsymbol{D} = [\boldsymbol{x}^{lb},\ \boldsymbol{x}^{ub}]. \end{aligned} \tag{LNG}$$

In Problem (LNG), $W_p(\boldsymbol{x})$ is the power consumption of unit p that is contained in compressors and pumps set, PM. $W_p(\boldsymbol{x})$ is given by the enthalpy change caused by the compression as if it was isentropic divided by the isentropic efficiency, η_c,

$$W_p = \frac{W_{p,ideal}}{\eta_c} = \frac{\left[H(Tout_{ideal}, Pout) - H(Tin, Pin) \right]}{\eta_c},$$

where $Tout_{ideal}$ is the temperature that provides equal entropy in the inlet and outlet streams ($S(Tin, Pin) - S(Tout_{ideal}, Pout) = 0$). For the SMR process, PM ={K-1, K-2, K-3, K-4, P-3, P-4}, and for the C3MR, PM ={K-1, K-2, K-3, K-4, K-101, K-102, K-103, K-104}. $UA_{ex}(x)$ is the global heat transfer coefficient multiplied by the area of the heat exchanger ex in the set of all heat exchangers HE, given by the heat exchanger duty, Q_{ex}, divided by the mean logarithmic temperature

Table 2
Search space bounds for the multi-objective optimization study.

$\boldsymbol{x}$	SMR			C3MR		
	$\boldsymbol{x}_{base}$	$\boldsymbol{x}^{lb}$	$\boldsymbol{x}^{ub}$	$\boldsymbol{x}_{base}$	$\boldsymbol{x}^{lb}$	$\boldsymbol{x}^{ub}$
m_N [kg h^{-1}]	0.250	0.000	0.375	0.200	0.000	0.300
m_{C1} [kg h^{-1}]	0.700	0.350	1.050	0.600	0.300	0.900
m_{C2} [kg h^{-1}]	1.000	0.500	1.500	1.000	0.500	1.500
m_{C3} [kg h^{-1}]	1.100	0.550	1.650	0.600	0.300	0.900
m_{iC5} [kg h^{-1}]	1.800	0.900	2.700	–	–	–
P_{suc} [kPa]	250.0	125.0	375.0	250.0	125.0	375.0
P_{dis} [kPa]	5000	2500	7500	5000	2500	7500
$T_{f,precool}$ [°C]	–	–	–	−35.00	−37.00	−30.00
T_{exp} [°C]	−40.00	−60.00	−20.00	−125.0	−135.0	−115.0

difference, ΔTml_{ex},

$$UA_{ex} = \frac{Q_{ex}}{\Delta Tml_{ex}}.$$

For the SMR process, HE ={MSHE-1, MSHE-2, C-1, C-2, C-3, C-4}, and for the C3MR, HE ={MSHE-1, MSHE-2, MSHE-100, C-1, C-2, C-3, C-4}. The cold utility used in the coolers {C-1, …, C-4} is considered to be at 30 °C. Notice that these calculations, jointly with the equation of state and flash calculations, are performed in the process simulator and these results are readily available to the user. The work consumption and UA values are divided by the mass flow rate of LNG, $\dot{m}_{LNG}$, to generalize the process energy consumption and heat conductance in terms of LNG production. Therefore, the total power consumption and UA are readily available for a different natural gas flow rate by multiplying the resulting LNG production by the respective specific values. $\boldsymbol{Th}_{\kappa}(\boldsymbol{x})$ and $\boldsymbol{Tc}_{\kappa}(\boldsymbol{x})$ are the temperatures of hot and cold composite curves in the κth segment of the MSHE-1 and MSHE-2, and Ω_{κ} is the set of the $N\ell$ points from composite curves calculations that belong to section κ [17]. These values are also readily available to the user in the "LNG Exchanger" unit operation of the Aspen HYSYS process simulator, which, to account for the nonlinear behavior of enthalpy with temperature, performs a temperature discretization in the hot and cold streams and assures energy balance in each temperature stage. Notice that the temperature driving force constraints are not required because it is already assured by setting the temperature of the cold streams 3 °C below the cold-end of the hot streams, as explained in Section 3.1.

As discussed in Section 3.1, there are eight decision variables in $\boldsymbol{x}$ for each process so $n = 8$. For the SMR process optimization, $\boldsymbol{x} = [m_{i\in REFR}, P_{suc}, P_{dis}, T_{exp}]$, in which $REFR$ = {nitrogen (N), methane (C_1), ethane (C_2), propane (C_3), i-pentane (iC_5)}. For the C3MR process optimization, $\boldsymbol{x} = [m_{i\in REFR}, P_{suc}, T_{f,precool}, P_{dis}, T_{exp}]$, in which $REFR$ = {nitrogen (N), methane (C_1), ethane (C_2), propane (C_3)}. $\boldsymbol{\mathcal{D}}$ contains the lower and upper limits for the decision variables ($\boldsymbol{x}^{lb}$ $\boldsymbol{x}^{ub}$), and $\dot{m}_{LNG}$ is the LNG mass flow rate produced. The upper and lower limits of $\boldsymbol{x}$ are reported in Table 2 for SMR and C3MR. These values are set to be between 50% below and above a heuristically determined base case, *i.e.* $[0.5\boldsymbol{x}_{base}, 1.5\boldsymbol{x}_{base}]$. These bounds are intended to include promising regions while avoiding unstable simulations convergence because of flowsheet configuration that is far beyond the feasible space. The lower bound of m_N is set to 0 to account for refrigerant mixtures without nitrogen. The final precooling and expansion temperatures are bounded heuristically.

4. Optimization framework

The present multi-objective simulation–optimization framework is presented in Algorithm 1. Also, a schematic illustration is introduced in Fig. 3 to improve the clarity of the presented algorithm as well as the connections between the pieces of software. This framework substitutes the black-box objectives and constraints functions with kriging models and employs the ε-constraint method to handle the competing objectives. The algebraic approximated optimization subproblems are embedded into a nonlinear programming problem and solved with CONOPT local solver in GAMS.

Algorithm 1: Kriging-based multi-objective optimization framework

Input: Initial sample size $m_0 \in \mathbb{N}_+$, maximum number of samples $m_f \in \mathbb{N}_+$, design space $\boldsymbol{\mathcal{D}} \in \mathbb{R}^{2\times n}$, a function to calculate $\boldsymbol{f}$ and $\boldsymbol{g}$ values for a $\boldsymbol{x} \in \boldsymbol{\mathcal{D}} \subseteq \mathbb{R}^n$, and the number of non-dominated solutions (ε-constraint values) $n_\varepsilon \in \mathbb{N}_+$

1) Generate m_0 samples $\mathbf{X}$ with respective simulation output values $\mathbf{Y} = [\boldsymbol{f}; \boldsymbol{g}]^{\intercal}$ and define $\mathbf{D}_0 = [\mathbf{X}\ \mathbf{Y}]$;
2) Solve the single-objective optimization problem for each $\boldsymbol{f}_i$, $i = 1, 2$:

$$\min_{\boldsymbol{x}\in\boldsymbol{\mathcal{D}}} \ f_i(\boldsymbol{x})$$
$$s.t. \ \ \boldsymbol{g}(\boldsymbol{x}) \le 0,$$

using kriging-based adaptive sampling procedure [17] to determine $\boldsymbol{x}_1^*$ and $\boldsymbol{x}_2^*$ (solutions of f_1 and f_2, respectively), with $\mathbf{D} = \mathbf{D}_0$, m_f, $\boldsymbol{\mathcal{D}}$, and $m \leftarrow m_0$:
while $m < m_f$ *and stall iterations* < 5 **do**
  2.1) Fit/Update kriging models for f_i and $\boldsymbol{g}$;
  2.2) Solve surrogate optimization problem in GAMS;
  2.3) Simulate at the surrogate solution, append new data $\mathbf{D}$, and iterate $m = m + 1$;
end
3) Define ε as the equally spaced n_ε-vector from $f_1(x_1^*)$ to $f_1(\boldsymbol{x}_2^*)$;
4) Append to the data: $\mathbf{D}_2 = \mathbf{D}_0 \cup [\boldsymbol{x}_1^*,\ \mathbf{f}(\mathbf{x}_1^*),\ \boldsymbol{g}(\boldsymbol{x}_1^*)] \cup [\boldsymbol{x}_2^*,\ \boldsymbol{f}(\boldsymbol{x}_2^*),\ \boldsymbol{g}(\boldsymbol{x}_2^*)]$];
for $ite = 3, \ldots, n_\varepsilon$ **do**
  5) Solve the Problem (ε-SO) with $\mathbf{D} = \mathbf{D}_{ite-1}$, m_f, $\boldsymbol{\mathcal{D}}$, and $m \leftarrow m_0 + ite - 1$:
  while $m < m_f$ *and stall iterations* < 5 **do**
    5.1) Fit/Update kriging models for $\boldsymbol{f}$ and $\boldsymbol{g}$;
    5.2) Solve Problem (ε-SO) in GAMS;
    5.3) Simulate at the surrogate solution, append new data $\mathbf{D}$, and iterate $m = m + 1$;
  end
  6) Append the solution to the data: $\mathbf{D}_{ite} = \mathbf{D}_{ite-1} \cup [\boldsymbol{x}_{ite}^*, \boldsymbol{f}(\boldsymbol{x}_{ite}^*), \boldsymbol{g}(\boldsymbol{x}_{ite}^*)]$;
end
7) Eliminate dominated and infeasible solutions from $\mathbf{D}_{n_\varepsilon}$ to form $\mathbf{P}$, the set of non-dominated solutions;
Output: Pareto solutions, $\mathbf{P}$.

The calculation of $\boldsymbol{f}$ and $\boldsymbol{g}$ at given $\boldsymbol{x}$ is achieved by a function written in MATLAB that connects to the process simulator Aspen HYSYS. This connection is via the MATLAB built-in function "actxserver" that exposes the Aspen HYSYS objects and functions to the programming environment. The values of $\boldsymbol{x}$ are set to the respective object property (stream or unit operation), and the $\boldsymbol{f}$ and $\boldsymbol{g}$ values are acquired after converging the simulation.

Step 1 of Algorithm 1 is to generate m_0 samples of $\mathbf{X}$. For that, the maximization of the sample points' minimum distance in the search space $\boldsymbol{\mathcal{D}}$ is performed, employing a Latin Hypercube algorithm. With programming and simulation environments connected, the value of $\boldsymbol{f}$ and $\boldsymbol{g}$ are calculated in the simulation for each $\boldsymbol{x} \in \mathbf{X}$. The initial data is defined as $\mathbf{D}_0 = [\mathbf{X}\ \mathbf{Y}]$.

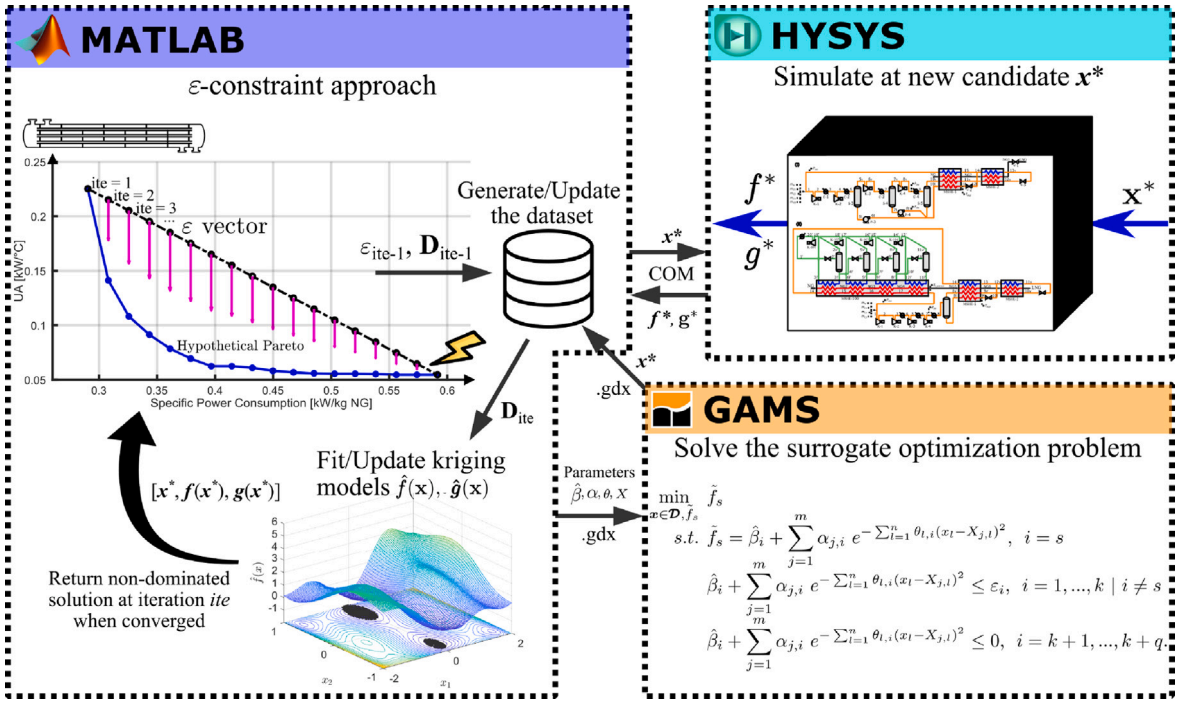

Fig. 3. Algorithmic building blocks of present multi-objective optimization framework based on kriging surrogate model.

Given $\mathbf{D}_0$, m_f, and $\mathcal{D}$, step 2 of Algorithm 1 is the single-objective optimization for each f_i objective, solved using the framework for constrained, black-box optimization proposed in Santos et al. [17]. It consists of using the data in D_0 to fit kriging models for the objective and constraints kriging-based adaptive sampling procedure (ε or regular ones). These models are implemented in a nonlinear programming problem in GAMS and solved with CONOPT gradient-based solver. The solution, which is a promising feasible and decreasing candidate, is evaluated in the simulation and the $\boldsymbol{x}$, f_i, and $\boldsymbol{g}$ values are attached to the dataset. The surrogate models are upgraded with the new data and this process is repeated until the surrogate problem optimization fails to provide an improving candidates five times or simulation evaluation budget m_f is reached. Talk about stopping criteria. The reader is invited to read Santos et al. [17] for more information on this algorithm and implementation.

The third step is to use the value of f_1 at the solutions of each single-objective problem, $f_1(\boldsymbol{x}_1^*)$ and $f_1(\boldsymbol{x}_2^*)$, to bound the ε vector. The ε-constraint vector is defined as the equally distributed n_ε-vector from $f_1(\boldsymbol{x}_1^*)$ to $f_1(\boldsymbol{x}_2^*)$. Fourth step consists of appending the single-objective solutions to the data $\mathbf{D}_2$. The subscript of $\mathbf{D}$ stands for the number of non-dominated solutions it already stores. In this case, it is two that account for the single-objective solutions. For the other entries of ε, the ε-constrained single-objective optimization in Problem (ε-SO) is solved using a slight modification of the aforementioned framework for constrained, black-box optimization proposed in Santos et al. [17]. The difference now is that the surrogate optimization problem includes the kriging-based ε-constrain for the f_1. Each optimization solution is appended to $\mathbf{D}_{ite-1}$, so that $\mathbf{D}_{ite} = \mathbf{D}_{ite-1} \cup [\boldsymbol{x}_{ite}^*, \boldsymbol{f}(\boldsymbol{x}_{ite}^*), \boldsymbol{g}(\boldsymbol{x}_{ite}^*)]$.

The last step of the proposed framework is to eliminate dominated and infeasible solutions from $\mathbf{D}_{n_\varepsilon}$, which contains the non-optimal initial data ($\mathbf{D}_0$) and possibly non-improving iterations from the algorithm. The new set, $\mathbf{P}$, is the Pareto Front as it only contains non-dominated solutions. In other words, the solutions that are infeasible $\boldsymbol{g}(\boldsymbol{x}) > 0$ are eliminated. Also, every solution that is dominated by another is eliminated, *i.e.* if there exists at least one $\boldsymbol{x}_j \in \mathbf{P}$ such that $f_i(\boldsymbol{x}_j) < f_i(\boldsymbol{x}_k)$ for all i, then $\boldsymbol{x}_k$ is dominated and eliminated. Notice that the data in $\mathbf{D}$ and, consequently, in the non-dominated solutions $\mathbf{P}$ are given by the rigorous simulation and not by the surrogates models. Therefore, the optimal natural gas liquefaction processes designed with Algorithm 1 would conform with rigorous thermodynamic and unit operation models, instead of surrogate approximations.

5. Results

The kriging-based multi-objective optimization approach is applied to the optimum design of SMR and C3MR processes for LNG production, considering $k = 2$ objectives of minimizing power consumption and heat exchanger area utilization. The optimization parameters are initial sample size $m_0 = 10n$, function evaluation budget $m_f = 20n$, number of decision variables $n = 8$, and number of sections into which each MSHE is divided $K = 10$. The number of non-dominated solutions is heuristically determined as the number of objectives times the size of the problem plus the number of objectives for the single optima: $n_\varepsilon = k \times n + k = 18$. The NSGA-II parameters are set to the default of the algorithm from the MATLAB optimization toolbox ("gamultobj"), except for individuals ($10n$) and generations (20) that are selected heuristically and to match the function evaluation budget of $20n$ for a fair comparison between algorithms. To account for the randomness of the initial sample in both approaches, each algorithm was run three times.

Fig. 4 illustrates the Pareto Front delimited by the non-dominated solutions achieved with the present framework as well as the NSGA-II algorithm. For both SMR and C3MR, the present Pareto Fronts dominate the meta-heuristics results. The optimal SMR processes have non-dominated solutions that present energy consumption as low as 1045 kJ/kg-LNG and specific *UA* value of 212.2 kJ/(°C kg-LNG). Meanwhile, the extreme solutions for NSGA-II are 1222 kJ/kg-LNG of energy consumption and specific *UA* value of 216.7 kJ/(°C kg-LNG). The non-dominated solutions of the C3MR process have energy consumption and specific *UA* as low as 980.3 kJ/kg-LNG and 266.9 kJ/(°C kg-LNG), while the NSGA-II have 1054 kJ/kg-LNG and 284.7 kJ/(°C kg-LNG). These results show that the present framework was also able to provide broader Pareto Fronts in the single-objectives directions. It can be inferred that the ranking method of dealing with competing objectives in population-based approaches was unable to spread the

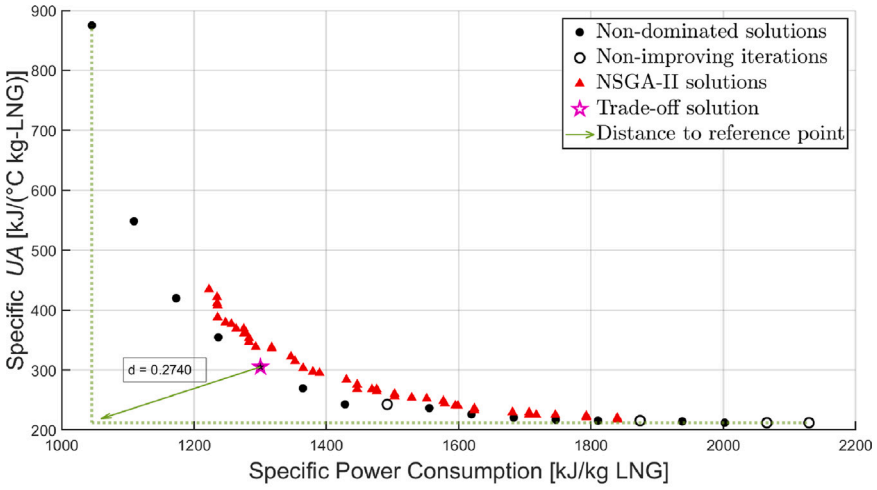

(a) SMR.

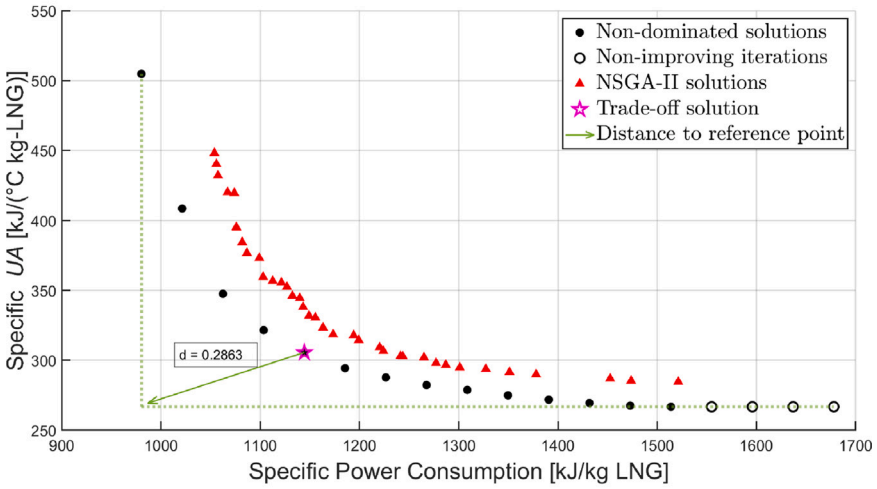

(b) C3MR.

Fig. 4. Non-dominated solutions from present approach and NSGA-II.

non-dominated solutions enough to reach close to the single-optimum solutions. Therefore, bounded objective function methods such as the ε-constraint with an appropriate single-objective optimization framework of the transformed multi-objective problem have shown to be more efficient. The limitations of the present approach are for many objectives, as the size of the ε vector grows quickly with the number of objectives.

The shape of these Pareto curves shows that the rate of change in the heat exchanger area with specific power consumption is more pronounced at low values of the latter. That is expected from the physical point-of-view because the heat exchanger area is roughly directly proportional to the inverse o the temperature differences between hot and cold composite curves. And, to achieve low power consumption, these temperature differences have to be very small, which makes its inverse (roughly area) explodes to high values. Based on that, an interesting trade-off solution would be not so small in power consumption because the *UA* values increase too quickly (high rate of change), but not so small on *UA* as it requires to increase power consumption too much (low rate of change). Trade-off solutions can be derived numerically from the Pareto curve in various ways [24]. In the case of heat exchanger area and power consumption objectives, a decision-maker could choose from the non-dominated solutions considering weight factors that take into account their costs and environmental impacts. However, these values are volatile and uncertain, requiring a more in-depth study for a single application. On the other hand, a simple, more robust, and yet good choice of non-dominated solution that balances high energy efficiency and heat exchanger area utilization is the one given by the reference point criterion [25]. This consists of choosing the non-dominated solution with smaller euclidean norm to a reference point in the objective function space. The reference point is here considered to be the minimum value of UA and power consumption ($[\min_{ii \in NS}(UA_{ii}), \min_{ii \in NS}(W_{ii})]$), such that where ts is the trade-off solution (see Eq. (6)), and NS is the set of non-dominated solutions. For both processes, these solutions are the fifth non-dominated one, which are highlighted in Fig. 4 with the magenta star. For the SMR process, the trade-off solution presents a 24.40% increase in work consumption and a 43.83% increase in *UA* compared to the energy and *UA* optima. For the C3MR process, it presents a 16.70% increase in work consumption and a 14.54% increase in *UA* compared to the energy and *UA* optima. For a further investigation of the process design point of view of these optimization results, Tables 3 and 4 present the decision variables, objectives, and constraints of the energy-optimum, *UA*-optimum, and the trade-off solution of SMR and C3MR, respectively.

From the multi-objective optimization results of the SMR process in Table 3, it is evident that the energy-optimum solution presents a greater mass flow rate of the heaviest components to achieve phase

$$ts = \arg\min_{i \in NS} \left\{ \sqrt{\left(\frac{W_i - \min_{ii \in NS}(W_{ii})}{\max_{ii \in NS}(W_{ii}) - \min_{ii \in NS}(W_{ii})} \right)^2 + \left(\frac{UA_i - \min_{ii \in NS}(UA_{ii})}{\max_{ii \in NS}(UA_{ii}) - \min_{ii \in NS}(UA_{ii})} \right)^2 } \right\} \quad (6)$$

Box I.

Table 3
Multi-objective optimization results for the SMR process for LNG production.

Decision variables results	Energy-optimum	UA-optimum	Trade-off solution
m_N [kg h^{-1}]	0.2566	0.1479	2.959E−02
m_{C1} [kg h^{-1}]	0.4407	0.7652	0.4209
m_{C2} [kg h^{-1}]	1.4170	1.141	0.9545
m_{C3} [kg h^{-1}]	0.7914	1.009	0.7317
m_{iC5} [kg h^{-1}]	1.842	1.175	1.410
P_{suc} [kPa]	338.7	125.0	125.0
P_{dis} [kPa]	3567	7500	5277
T_{exp} [°C]	−27.43	−20.00	−60.00
Objective functions and constraints summary			
Net work consumption $\left[\frac{\text{kJ}}{\text{kg NG}}\right]$	1045	2001	1300
Specific UA $\left[\frac{\text{kJ}}{\text{°C kg LNG}}\right]$	874.9	212.2	305.2
MSHE-1 minimum temperature approach [°C]	3.009	15.13	3.897
MSHE-2 minimum temperature approach [°C]	3.009	7.726	3.006
Detailed Results			
W_{K-1} $\left[\frac{\text{kJ}}{\text{kg NG}}\right]$	281.1	512.7	349.8
W_{K-2} $\left[\frac{\text{kJ}}{\text{kg NG}}\right]$	296.5	568.5	377.7
W_{K-3} $\left[\frac{\text{kJ}}{\text{kg NG}}\right]$	251.7	513.5	330.5
W_{K-4} $\left[\frac{\text{kJ}}{\text{kg NG}}\right]$	207.6	392.0	229.3
W_{P-3} $\left[\frac{\text{kJ}}{\text{kg NG}}\right]$	4.870	0.000	1.489
W_{P-4} $\left[\frac{\text{kJ}}{\text{kg NG}}\right]$	3.499	14.60	11.29
UA_{MSHE-1} $\left[\frac{\text{kJ}}{\text{°C kg LNG}}\right]$	354.7	39.70	125.1
UA_{MSHE-2} $\left[\frac{\text{kJ}}{\text{°C kg LNG}}\right]$	438.6	83.25	106.5
UA_{C-1} $\left[\frac{\text{kJ}}{\text{°C kg LNG}}\right]$	13.26	15.46	12.91
UA_{C-2} $\left[\frac{\text{kJ}}{\text{°C kg LNG}}\right]$	26.25	18.90	15.86
UA_{C-3} $\left[\frac{\text{kJ}}{\text{°C kg LNG}}\right]$	24.24	30.35	28.43
UA_{C-4} $\left[\frac{\text{kJ}}{\text{°C kg LNG}}\right]$	17.77	24.27	16.35

separation so that the liquid phase is the most responsible for the cooling task down to T_{exp} of −27.43 °C in MSHE-1. This helps save power consumption in the compressors. Also, the overall pressure ratio of 10.53 is the smallest among the three non-dominated solutions analyzed in this table. The *UA*-optimum solution presents an LNG process configuration that exploits high pressure ratio (60) of the refrigeration cycle to increase the temperature difference between hot and cold composite curves in the MSHEs to diminish their heat transfer area. The composition and flow rate of the multi-component refrigerant are also determined by the optimization approach to maintaining the high-temperature driving force throughout the MSHEs, as the power consumption is not been taken care of. The trade-off solution presents an intermediate cycle pressure ratio (42.22) compared to the other two solutions. The amount of heavy component (iso-pentane) in the mixed refrigerant is also in-between values of single-objective optima. The same behavior can be observed in the multi-objective optimization results of the C3MR process in Table 4. The overall cycle pressure ratio goes from 12.63 to 32.13, and finally to 59.57 for energy-optimum, trade-off solution, and *UA*-optimum, respectively. The detailed results of specific $W_{p \in PM}$ in Tables 3 and 4 show that the power consumption in the mixed-refrigerant cycle follows the net power consumption trend. On the other hand, the compressors of the propane cycle consume the most energy for the energy-optimum solution, which is counter-intuitive. The mixed-refrigerant for this solution is richer in heavier components (ethane and propane) so it requires more propane heat sink and, consequently, more compression power. That pays off with smaller overall pressure ratio as explained above. The detailed results of specific $UA_{ex \in HE}$ in Tables 3 and 4 present clearly that the main contributors for diminishing or augmenting the overall heat transfer area utilization are the MSHE-1 and MSHE-2. Therefore, the overall *UA* is mostly dependent on the mixed-refrigerant composition and flow rate, even for the C3MR process.

Apart from the design variables analyzed in the previous paragraph, the other variables do not present an intermediate relationship between

Table 4
Multi-objective optimization results for the C3MR process for LNG production.

Decision variables results	Energy-optimum	UA-optimum	Trade-off solution
m_N [kg h^{-1}]	2.523E−02	0.2106	2.052E−02
m_{C1} [kg h^{-1}]	0.4079	0.6017	0.4187
m_{C2} [kg h^{-1}]	0.8983	0.6884	0.7393
m_{C3} [kg h^{-1}]	0.5550	0.4725	0.5482
P_{suc} [kPa]	2.387	125.9	130.0
P_{dis} [kPa]	3014	7500	4177
$T_{f,precool}$ [°C]	−37.00	−36.98	−37.00
T_{exp} [°C]	−122.2	−134.7	−135.0
Objective functions and constraints summary			
Net work consumption $\left[\frac{kJ}{kg\ NG}\right]$	980.3	1518	1144
Specific UA $\left[\frac{kJ}{°C\ kg\ LNG}\right]$	508.3	266.9	305.7
MSHE-1 minimum temperature approach [°C]	3.010	5.647	3.009
MSHE-2 minimum temperature approach [°C]	3.011	9.702	3.039
Detailed Results			
W_{K-1} $\left[\frac{kJ}{kg\ NG}\right]$	125.9	245.1	166.5
W_{K-2} $\left[\frac{kJ}{kg\ NG}\right]$	145.1	313.1	201.9
W_{K-3} $\left[\frac{kJ}{kg\ NG}\right]$	165.3	330.1	225.7
W_{K-4} $\left[\frac{kJ}{kg\ NG}\right]$	162.5	304.2	207.6
W_{K-101} $\left[\frac{kJ}{kg\ NG}\right]$	158.5	140.4	147.7
W_{K-102} $\left[\frac{kJ}{kg\ NG}\right]$	111.2	93.34	102.3
W_{K-103} $\left[\frac{kJ}{kg\ NG}\right]$	76.80	61.94	62.65
W_{K-104} $\left[\frac{kJ}{kg\ NG}\right]$	34.89	30.21	29.90
UA_{MSHE-1} $\left[\frac{kJ}{°C\ kg\ LNG}\right]$	269.1	55.62	94.67
UA_{MSHE-2} $\left[\frac{kJ}{°C\ kg\ LNG}\right]$	25.08	3.792	6.263
$UA_{MSHE-100}$ $\left[\frac{kJ}{°C\ kg\ LNG}\right]$	116.7	102.6	104.5
UA_{C-1} $\left[\frac{kJ}{°C\ kg\ LNG}\right]$	0.000	8.521	5.354
UA_{C-2} $\left[\frac{kJ}{°C\ kg\ LNG}\right]$	7.215	10.15	7.995
UA_{C-3} $\left[\frac{kJ}{°C\ kg\ LNG}\right]$	7.985	12.27	9.098
UA_{C-4} $\left[\frac{kJ}{°C\ kg\ LNG}\right]$	82.14	73.91	77.80

energy and *UA* optima. In other words, the non-dominated solutions are not fine-tuned interpolations of single-objective ones. This interesting finding shows the capability of a multi-objective optimization framework to determine complex and unique non-dominated solutions forming a Pareto curve for a decision-maker to choose from. Therefore, the importance of multi-objective optimization approaches to design problems with competing objectives is determining the rate of change of one objective with the other and deriving trade-off solutions that are not mere adjusted interpolations of single-objective ones. The same quality of trade-off analysis would not be possible by simply using single-objective optimization of a function that weights the competing objectives.

Another important use of the multi-objective optimization approach is to serve as a tool for helping to decide among technologies. Fig. 5 illustrates a comparison between the SMR and C3MR liquefaction processes based on specific power consumption and heat exchange area utilization. Given economic and industrial site scenarios, it would be readily possible to determine which is the natural gas liquefaction technology most suited considering the price of electricity, installed power, heat exchanger costs, and available plant site area. For the given natural gas conditions and process considerations, the C3MR solutions dominate the SMR ones up to around 1355 kJ/kg-LNG of specific power consumption and 274.5 kJ/(°C kg-LNG) of specific *UA*. It means that, if energy consumption is required to be below this value, the C3MR natural gas liquefaction process should be employed. However, if the overall *UA* value is expected to be smaller than 274.5 kJ/(°C kg-LNG), then the SMR process should be selected. This inflection point that separates the dominance between C3MR and SMR in objectives functions space is drawn in Fig. 5 with the blue point. All-in-all, C3MR processes are more energetically efficient for flexible heat exchanger area utilization, whereas SMR processes are more energetically efficient for strict heat exchanger area utilization. SMR processes can achieve small values of *UA* that C3MR cannot, while the former can achieve small values of power consumption that the latter cannot.

Comparing the optimization results with the literature is challenging because the different author uses different process considerations such as natural gas pressure, temperature, and composition, compressors and pumps efficiency, pressure drop in heat exchangers, LNG specifications, cooling temperature, and process constraints. Table 5 presents the literature results of natural gas liquefaction processes optimized to minimize the specific power consumption that considered the same parameters and considerations presented in Table 1. These results show the competitiveness of the kriging-based that surpassed the recent literature, except for the SMR proposed by Qyyum et al. [26]. They included hydraulic turbines in the refrigeration cycle instead of Joule–Thomson valves, which increases the energy efficiency but is not conclusive

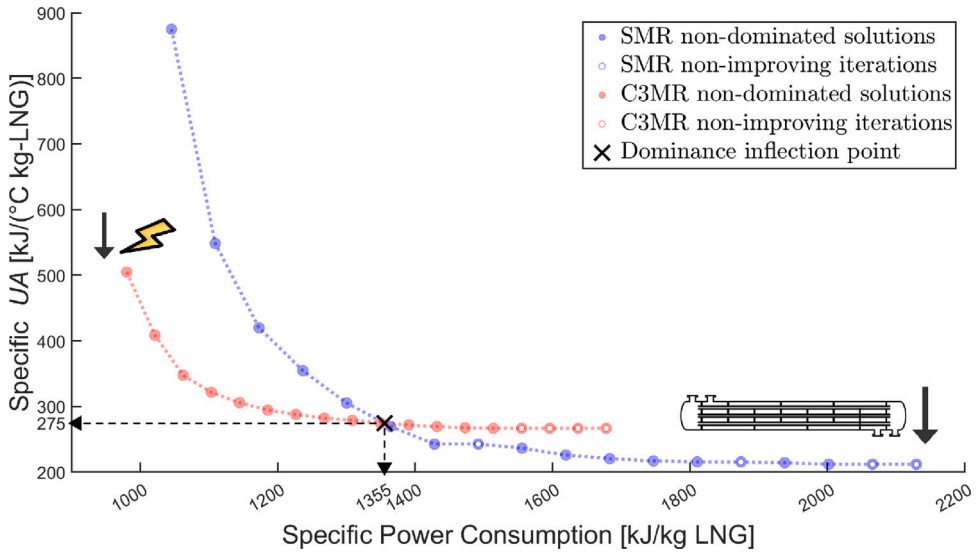

Fig. 5. SMR and C3MR Pareto Fronts comparison.

Table 5
Comparison with literature results on energy-optimum natural gas liquefaction processes.

	Khan et al. [27]		Khan et al. [22]		Qyyum et al. [26]		Ali et al. [28]	Ali et al. [29]	Majeed et al. [30]		Present work	
LNG technology	SMR	C3MR	SMR	C3MR	SMR	SMR[a]	SMR	SMR	SMR	C3MR	SMR	C3MR
Power $\left[\frac{kJ}{kg\ \ LNG}\right]$	1557	1002	1709	1021	1344	1019	1665	14315	1444	1017	1045	980
MITA [°C]	3.010	3.000	3.003	3.015	3.000	3.000	2.813	2.640	3.000	3.000	3.009	3.011
Decision Variables												
m_N [kg h^{-1}]	0.2276	0.0395	0.2690	0.0900	0.2590	0.0700	0.3219	0.2424	0.1650	0.0800	0.2566	0.0252
m_{C1} [kg h^{-1}]	0.5343	0.4223	0.5290	0.5130	0.4630	0.4780	0.4665	0.5124	0.4630	0.4490	0.4407	0.4079
m_{C2} [kg h^{-1}]	0.6312	0.6455	0.6190	0.8300	0.7660	0.5110	0.7210	0.5260	0.6360	0.8430	1.4170	0.8983
m_{C3} [kg h^{-1}]	2.7280	0.6800	2.8470	0.5320	2.2670	1.8190	2.8265	2.9022	2.2880	0.5690	0.7914	0.5550
m_{iC5} [kg h^{-1}]	–	–	–	–	–	–	–	–	–	–	1.842	–
P_{suc} [kPa]	–	–	–	3.30	2.03	2.60	–	–	1.55	2.75	3.39	2.39
P_{dis} [kPa]	49.97	46.50	48.00	50.00	62.49	78.90	48.34	45.57	59.50	43.43	35.67	30.14
T_{NG2} [°C]	–	–	–	22.40	–	–	–	–	–	18.40	–	–
T_{NG3} [°C]	–	–	–	4.00	–	–	–	–	–	0.00	–	–
T_{NG4} [°C]	–	–	–	−14.00	–	–	–	–	–	−16.75	–	–
$T_{f,precool}$ [°C]	–	–	–	–	–	–	–	–	–	–	–	−37.00
T_{exp} [°C]	–	–	−155.00	−133.40	–	–	−159.26	−152.97	–	–	−27.43	−122.20

[a]Replaced Joule–Thomson valves with hydraulic turbines.

without an economic assessment. Therefore, these results provide a flavor of the quality of the processes designed in this paper using the kriging-based multi-objective approach.

6. Conclusions

This paper presented an application of a kriging-based optimization framework to solve constrained, black-box, multi-objective, simulation–optimization problem of the optimal design of SMR and C3MR natural gas liquefaction processes, considering the minimization of both power consumption and heat exchanger area utilization and using a reliable process simulator. The framework is based on fitting kriging models to simulation data to substitute the black-box objectives and constraints with a simple algebraic formulation. The ε-constraint methodology is employed to reformulate the multi-objective problem into several single-objective ones. The surrogate, single-objective optimization sub-problems are solved in GAMS with CONOPT solver to provide a sampling tool of promising feasible and non-dominated solutions to the original problem.

The Pareto Fronts determined by the present approach to the SMR and C3MR processes dominate the ones achieved with well-established multi-objective meta-heuristics of NSGA-II and are also broader in the single-objective directions. The objective functions of non-dominated solutions go as low as 1045 kJ/kg-LNG and specific *UA* value of 212.2 kJ/(°C kg-LNG) for SMR and 980.3 kJ/kg-LNG and 266.9 kJ/(°C kg-LNG) for C3MR. The trade-off solutions that present the minimum sum of relative objectives were analyzed. These trade-off results balance the objectives by a 24.40% increase in work consumption and a 43.83% increase in *UA* for the SMR process and a 16.70% increase in work consumption and a 14.54% increase in *UA* for the C3MR process, compared to the energy and *UA* optima. The comparison of Pareto solutions of the SMR and C3MR processes showed that the C3MR solutions dominate the SMR ones up to around 1355 kJ/kg-LNG of

specific power consumption and 274.5 kJ/(°C kg-LNG) of specific *UA*. This finding provides a numerical metric for choosing between the C3MR, which is suitable for energetically efficient applications, and the SMR, which is more appropriate for restricted heat exchanger area utilization. A comparison of optimal LNG processes with previous works showed the competitiveness of the kriging-based that surpassed the recent literature.

The importance of multi-objective optimization approaches to design problems with competing objectives is determining the rate of change of one objective with another, deriving complex trade-off solutions that are not mere adjusted interpolations of single-objective ones, and providing a more thorough and robust platform to compare among choices with competing objectives. For the case of natural gas liquefaction process design, it allowed deriving promising SMR and C3MR solutions that balance power consumption and heat transfer area utilization. Also, an inflection point in the objective space is observed. This point separates dominance between C3MR and SMR processes, making it easier for a decision-maker to choose the appropriate technology for specific scenarios.

Declaration of competing interest

The authors declare that they have no known competing financial interests or personal relationships that could have appeared to influence the work reported in this paper.

Data availability

Data will be made available on request.

Acknowledgments

The authors LFS, CBBC, and MASSR acknowledge the National Council for Scientific and Technological Development–CNPq (Brazil), processes 200305/2020-4, 148184/2019-7, 440047/2019-6, 311807/2018-6, 428650/2018-0, 307958/2021-3 and Coordination for the Improvement of Higher Education Personnel–CAPES (Brazil) for the financial support. The author JAC acknowledges financial support from the "Generalitat Valenciana, Spain" under project PROMETEO 2020/064 and the Ministerio de Ciencia e Innovación, Spain, under project PID2021-124139NB-C21.

References

[1] Kamath RS, Biegler LT, Grossmann IE. Modeling multistream heat exchangers with and without phase changes for simultaneous optimization and heat integration. AIChE J 2012;58(1):190–204. http://dx.doi.org/10.1002/aic.12565.

[2] Nagesh Rao H, Karimi IA. A superstructure-based model for multistream heat exchanger design within flow sheet optimization. AIChE J 2017;63(9):3764–77. http://dx.doi.org/10.1002/aic.15714.

[3] Watson HA, Vikse M, Gundersen T, Barton PI. Optimization of single mixed-refrigerant natural gas liquefaction processes described by nondifferentiable models. Energy 2018;150:860–76. http://dx.doi.org/10.1016/j.energy.2018.03.013.

[4] Boukouvala F, Floudas CA. ARGONAUT: AlgoRithms for global optimization of coNstrAined grey-box computational problems. Optim Lett 2017;11(5):895–913. http://dx.doi.org/10.1007/s11590-016-1028-2.

[5] Caballero JA, Grossmann IE. An algorithm for the use of surrogate models in modular flowsheet optimization. AIChE J 2008;54(10):2633–50. http://dx.doi.org/10.1002/aic.11579.

[6] Khan MS, Karimi I, Wood DA. Retrospective and future perspective of natural gas liquefaction and optimization technologies contributing to efficient LNG supply: A review. J Natural Gas Science Eng 2017;45:165–88. http://dx.doi.org/10.1016/j.jngse.2017.04.035.

[7] Qyyum MA, Qadeer K, Lee M. Comprehensive review of the design optimization of natural gas liquefaction processes: Current status and perspectives. Ind Eng Chem Res 2018;57(17):5819–44. http://dx.doi.org/10.1021/acs.iecr.7b03630.

[8] Austbø B, Løvseth SW, Gundersen T. Annotated bibliography—Use of optimization in LNG process design and operation. Comput Chem Eng 2014;71(12):391–414. http://dx.doi.org/10.1016/j.compchemeng.2014.09.010.

[9] Austbø B, Gundersen T. Impact of problem formulation on LNG process optimization. AIChE J 2016;62(10):3598–610. http://dx.doi.org/10.1002/aic.15266.

[10] Khan MS, Karimi I, Lee M. Evolution and optimization of the dual mixed refrigerant process of natural gas liquefaction. Appl Therm Eng 2016;96:320–9. http://dx.doi.org/10.1016/j.applthermaleng.2015.11.092.

[11] Deb K, Pratap A, Agarwal S, Meyarivan T. A fast and elitist multiobjective genetic algorithm: NSGA-II. IEEE Trans Evol Comput 2002;6(2):182–97. http://dx.doi.org/10.1109/4235.996017.

[12] Ghorbani B, Hamedi M-H, Shirmohammadi R, Hamedi M, Mehrpooya M. Exergoeconomic analysis and multi-objective Pareto optimization of the C3MR liquefaction process. Sustain Energy Technol Assess 2016;17:56–67. http://dx.doi.org/10.1016/j.seta.2016.09.001.

[13] Song R, Cui M, Liu J. Single and multiple objective optimization of a natural gas liquefaction process. Energy 2017;124:19–28. http://dx.doi.org/10.1016/j.energy.2017.02.073.

[14] Nguyen T-V, Rothuizen ED, Markussen WB, Elmegaard B. Thermodynamic comparison of three small-scale gas liquefaction systems. Appl Therm Eng 2018;128:712–24. http://dx.doi.org/10.1016/j.applthermaleng.2017.09.055.

[15] Primabudi E, Morosuk T, Tsatsaronis G. Multi-objective optimization of propane pre-cooled mixed refrigerant (C3MR) LNG process. Energy 2019;185:492–504. http://dx.doi.org/10.1016/j.energy.2019.07.035.

[16] Mofid H, Jazayeri-Rad H, Shahbazian M, Fetanat A. Enhancing the performance of a parallel nitrogen expansion liquefaction process (NELP) using the multi-objective particle swarm optimization (MOPSO) algorithm. Energy 2019;172:286–303. http://dx.doi.org/10.1016/j.energy.2019.01.087.

[17] Santos LF, Costa CB, Caballero JA, Ravagnani MA. Framework for embedding black-box simulation into mathematical programming via kriging surrogate model applied to natural gas liquefaction process optimization. Appl Energy 2022;310:118537. http://dx.doi.org/10.1016/j.apenergy.2022.118537.

[18] Sacks J, Welch WJ, Mitchell TJ, Wynn HP. Design and analysis of computer experiments. Statist Sci 1989;4(4):409–23. http://dx.doi.org/10.1214/ss/1177012413.

[19] Santos LF, Costa CB, Caballero JA, Ravagnani MA. Kriging-assisted constrained optimization of single-mixed refrigerant natural gas liquefaction process. Chem Eng Sci 2021;241:116699. http://dx.doi.org/10.1016/j.ces.2021.116699.

[20] Haimes YY, Lasdon LS, Wismer DA. On a bicriterion formulation of the problems of integrated system identification and system optimization. IEEE Trans Syst Man Cybern 1971;1(3):296–7. http://dx.doi.org/10.1109/TSMC.1971.4308298.

[21] Marler RT, Arora JS. Survey of multi-objective optimization methods for engineering. Struct Multidiscip Optim 2004;26(6):369–95. http://dx.doi.org/10.1007/s00158-003-0368-6.

[22] Khan MS, Karimi I, Bahadori A, Lee M. Sequential coordinate random search for optimal operation of LNG (liquefied natural gas) plant. Energy 2015;89:757–67. http://dx.doi.org/10.1016/j.energy.2015.06.021.

[23] Pham TN, Long NVD, Lee S, Lee M. Enhancement of single mixed refrigerant natural gas liquefaction process through process knowledge inspired optimization and modification. Appl Therm Eng 2017;110:1230–9. http://dx.doi.org/10.1016/j.applthermaleng.2016.09.043.

[24] Wang Z, Rangaiah GP. Application and analysis of methods for selecting an optimal solution from the Pareto-optimal front obtained by multiobjective optimization. Ind Eng Chem Res 2017;56(2):560–74.

[25] Deb K, Sundar J. Reference point based multi-objective optimization using evolutionary algorithms. In: Proceedings of the 8th annual conference on genetic and evolutionary computation. 2006, p. 635–42.

[26] Qyyum MA, Ali W, Long NVD, Khan MS, Lee M. Energy efficiency enhancement of a single mixed refrigerant LNG process using a novel hydraulic turbine. Energy 2018;144:968–76. http://dx.doi.org/10.1016/j.energy.2017.12.084.

[27] Khan MS, Lee M. Design optimization of single mixed refrigerant natural gas liquefaction process using the particle swarm paradigm with nonlinear constraints. Energy 2013;49(1):146–55. http://dx.doi.org/10.1016/j.energy.2012.11.028.

[28] Ali W, Khan MS, Qyyum MA, Lee M. Surrogate-assisted modeling and optimization of a natural-gas liquefaction plant. Comput Chem Eng 2018;118:132–42. http://dx.doi.org/10.1016/j.compchemeng.2018.08.003.

[29] Ali W, Qyyum MA, Khan MS, Duong PLT, Lee M. Knowledge-inspired operational reliability for optimal LNG production at the offshore site. Appl Therm Eng 2019;150:19–29.

[30] Majeed K, Qyyum MA, Nawaz A, Ahmad A, Naqvi M, He T, et al. Shuffled complex evolution-based performance enhancement and analysis of cascade liquefaction process for large-scale LNG production. Energies 2020;13(10):2511.